Title	Correlation between temperature distribution and changes in self-organized luminous pattern in an atmospheric pressure DC glow discharge with sheath gas flow
Author(s)	Miyazaki, Toshiaki; Sasaki, Koichi; Shirai, Naoki
Citation	Plasma Sources Science and Technology, 33(11), 115007 https://doi.org/10.1088/1361-6595/ad8c7b
Issue Date	2024-11-12
Doc URL	https://hdl.handle.net/2115/96186
Rights	This is the Accepted Manuscript version of an article accepted for publication in Plasma Sources Science and Technology. IOP Publishing Ltd is not responsible for any errors or omissions in this version of the manuscript or any version derived from it. The Version of Record is available online at https://doi.org/10.1088/1361-6595/ad8c7b.
Rights(URL)	https://creativecommons.org/licenses/by-nc-nd/4.0/
Type	journal article
File Information	2024miyazaki_psst.pdf

Correlation between temperature distribution and changes in self-organized luminous pattern in an atmospheric pressure DC glow discharge with sheath gas flow

Toshiaki Miyazaki, Koichi Sasaki and Naoki Shirai

Division of Applied Quantum Science and Engineering, Hokkaido University, Japan

E-mail: shun_me77@eis.hokudai.ac.jp

E-mail: nshirai@qe.eng.hokudai.ac.jp

June 2024

Abstract. The self-organized luminous patterns observed above the anode surface in atmospheric-pressure DC glow discharges were changed by the composition of the gas flow. The patterns were observed not only with liquid anodes but also with metal anodes. Various pattern structures were observed by changing the helium gas flow rate in the core and the ambient oxygen gas flow rate supplied during the discharge. When the pattern formation was observed, the emission spectra and the radial spread of the positive column changed, and the voltage-current characteristic also changed. These results suggest that not only the anode surface but the entire discharge affects the pattern formation. Comparing the results for the liquid and metal anodes, the trends in the pattern formation and voltage-current characteristics were almost identical. The gas temperature in the discharge was also investigated in two different ways, by the LIF of OH radicals and by Rayleigh scattering, and these two results were in good agreement. Under the condition where the pattern formed, the gas temperature in the discharge was approximately 2500-3000 K and higher than that of the discharge without the pattern formation. Focusing on the gradient of the temperature distribution, the discharge with the pattern formation had a steeper gradient than that of the discharge without the pattern formation. It was suggested that not only the high temperature of the discharge but also the large gradient of the temperature change plays an important role in the pattern formation. The role of oxygen gas in the pattern formation may be the effect of increasing the temperature and altering the temperature gradient in the discharge rather than generating negative ions in the discharge.

1. Introduction

Plasma-liquid interaction has attracted much attention for various applications [1, 2]. We have studied discharge plasmas with liquid which works as the electrode [3–5]. In particular, self-organized luminous pattern on the water surface is observed under certain conditions when the discharge is generated with liquid as the anode [6, 7]. The pattern formation observed with plasma generation has attracted much attention lately, and Trelles [8] and Foster [9] published review papers about this phenomenon in 2016 and 2019, respectively. We reported that oxygen gas has a significant effect on the pattern formation [7]. Therefore, we assumed that negative ions in the plasma would have a significant effect because oxygen gas is one of the electro-negative gases.

In general, every self-organized pattern formation can be described mathematically using "the reaction-diffusion system" proposed by A. Turing [10]. The reaction-diffusion system is a mathematical model that needs two variables called "activator" and "inhibitor". The relationship between the activator and the inhibitor are competitive, *i.e.*, the growth and the decay of the activator result in the decay and the growth of the inhibitor, respectively. We can find the works based on the reaction-diffusion system in different research fields such as the patterns of animals [11–13], the action potential changes in neurons [14,15], the structure of molecules [16], and the concentration changes in solution chemistry [17, 18]. The luminous patterns observed in plasmas can also be described by the reaction-diffusion system. For example, Rumbach and coworkers constructed a two-dimensional model, by which they reproduced the luminous pattern experimentally observed in a plasma generated in ambient air [19]. In their model, they assumed that the densities of electrons and positive ions are the two variables in the reaction-diffusion system, and the radial electric field in the thin sheath above the liquid anode induces the increase and the decrease in the two variables. On the other hand, Bieniek and coworkers used a mathematical model based on a first principle which are equations of similar form as the reaction-diffusion system, and simulated the patterns that appeared above the anode of a DC glow discharge [20]. Their calculation conditions were at a low-pressure (5 Torr) and in a pure helium gas atmosphere, and simulation studies have shown that self-organized pattern formations can be observed using only noble gases. The self-organized pattern formation has also been observed in DC discharges in other low-pressure environments using only noble gases, which suggests that negative ions may not necessarily be necessary to form the pattern. Other studies also reported that the pattern formation can be observed even in an atmosphere composed of only noble gases within a certain pressure range in low-pressure plasmas [21–23]. Since the neutral particle number density is lower in low-pressure environments than in atmospheric pressure, when the pattern is formed in atmospheric pressure plasma, there may be a decrease in the particle number density due to temperature increase, which means the particle number density and temperature in plasmas may be important parameters.

In many experiments on the self-organized pattern formation in DC discharge generated at atmospheric-pressure, the anodes are liquids [6, 7, 24–35], but the pattern formations above metal anodes are also reported [36, 37]. In both the cases of the liquid and metal anodes, the patterns are formed just above the anode surfaces, and they are never formed above the cathodes. Various patterns such as dots, rings, and spokes have been observed, and they are moving or stationary. It has been also reported to date that the pattern formation depends on the experimental conditions, such as the discharge current, the distance between the anode and the cathode, the gas composition, the conductivity of the electrodes, and the surface condition of the anode [7, 29, 38–40]. In addition, it has been found that electro-negative gases such as water vapor and oxygen gas play an important role in the pattern formation, and several authors point out the importance of electro-negative gases for the pattern formation [7, 26]. These discharge parameters and the ratio of electro-negative gases in and around the discharge are expected to affect the pattern formation by changing the reaction and diffusion in the reaction-diffusion system. Many papers investigated the effect of the discharge parameters on the pattern formation, but few papers investigated other effects such as oxygen gas or physical quantities, for example, gas number density and gas temperature. Only one paper we reported has discussed the significant effect of oxygen gas on the pattern formation. Therefore, it is unclear whether the effect of oxygen gas is due to negative ions or others, and it is also unclear how much oxygen must be present in the plasma to affect the pattern formation. To understand the mechanism of the pattern formation in the atmospheric-pressure DC glow discharge, it is important to investigate the effects of oxygen gas and physical quantities in plasma as well as discharge parameters on the pattern formation.

In this study, we investigated the influence of oxygen gas and gas temperature on the pattern formation. The composition of the gas was controlled by changing the flow rate of the helium gas flow that forms the core of the discharge plasma and the surrounding oxygen (or nitrogen) sheath gas. The gas temperature was investigated in two different ways using laser fluorescence spectroscopy of OH radicals and Rayleigh scattering. We report that the luminous pattern can be changed by using the presence of oxygen sheath gas around the discharge and that the gas temperature has important information about conditions of the pattern formation.

2. Experimental methods

Figure 1 shows the experimental setup for producing an atmospheric-pressure DC glow discharge with a miniature helium flow. A brass tube with an inner diameter of 500 μm, which worked as a gas nozzle, was used for the cathode. 1 % NaCl aqueous solution was used for the liquid anode, and helium gas was flowed from the nozzle toward the surface of the liquid anode. A stainless steel metal rod with a diameter of 20 mm was also used for the metal anode. A DC high voltage was applied between the anode and the nozzle cathode. The distances between the liquid anode and the nozzle cathode were 10 or 12 mm. The discharge was generated basically in ambient air, and a sheath nitrogen or oxygen gas was flowed around the helium gas flow to control the ambient gas atmosphere. The diameter of the nozzle for the sheath gas was 12 mm. Figure 2 shows examples when the discharge is generated (a)in ambient air, (b)with nitrogen sheath gas and (c)with oxygen sheath gas, respectively. The pattern forms in (a)in ambient air and (c)with oxygen sheath gas, but the pattern never forms in (b)with nitrogen sheath gas. In this work, the discharge current was changed between 20-80 mA, and the flow rates of helium gas and the nitrogen or oxygen sheath gas were 150-400 and 1000-2000 sccm, respectively.

To measure the gas temperature inside and around the discharge, we used laser-induced fluorescence spectroscopy (LIF) of OH radicals for measuring the rotational temperature distribution of OH radicals in the gas phase. This is because rotational temperature and gas temperature are approximately equal under atmospheric pressure. The LIF system was basically the same as that in our previous papers [41–43]. A pulsed laser beam which was yielded from a tunable dye laser was injected into the discharge column from the radial direction, as shown in Fig. 1(a). The wavelength of the dye laser was 261.50 nm, by which OH radicals at the ground state $[X^2\Pi(v''=0)]$ were excited to the $A^2\Sigma^+(v'=2)$ state. The laser energy was 5.0 mJ/pulse. The shape of the laser beam was arranged to be planar to illuminate the discharge area uniformly. We detected the fluorescences of the $\Delta v = 0$ transitions from $A^2\Sigma^+(v'=2)$, $A^2\Sigma^+(v'=1)$, and $A^2\Sigma^+(v'=0)$. The $A^2\Sigma^+(v'=1)$ and $A^2\Sigma^+(v'=0)$ states were produced by vibrational energy transfer. The fluorescence image was captured using a charge-coupled device camera with a gated image intensifier (ICCD camera) from the right angle to the laser beam. We examined the distributions of the rotational temperature of $OH(X^2\Pi(v=0))$ and the rotational temperature was obtained from the fluorescence intensities observed by the excitations of different rotational states of $OH(X^2\Pi(v=0))$.

However, the temperature distribution measurement by LIF can only measure the rotational temperature in a limited region where OH radicals are present. Therefore, we also used Rayleigh scattering to investigate temperatures in a wider region, as well as to cross-check our LIF results. The arrangement of the discharge, laser beam, and ICCD camera was the same as in the LIF measurement. The pulsed laser beam was yielded from an SHG light of Nd:YAG laser, and the laser wavelength and energy were 532 nm and 10 mJ/pulse, respectively. The laser beam was focused by a focal length f=20 cm lens and irradiated into the discharge, and the Rayleigh scattered light was measured by the ICCD camera as an image. From the relation p=nkT (where k is Boltzmann's constant) for pressure p, number density n of gas particles, and gas temperature T, if pressure p is constant at atmospheric pressure, number density n and temperature T are inversely proportional to each other. Since the signal intensity from Rayleigh scattered light is proportional to the gas density n, the temperature T was estimated from the inverse ratio of the Rayleigh scattering signal intensity.

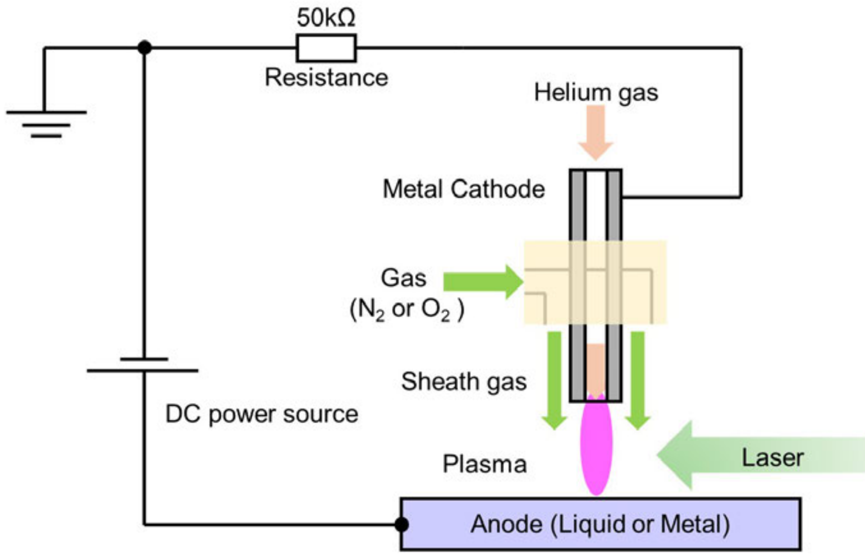

Figure 1. Experimental setup for generating atmospheric-pressure DC glow discharge.

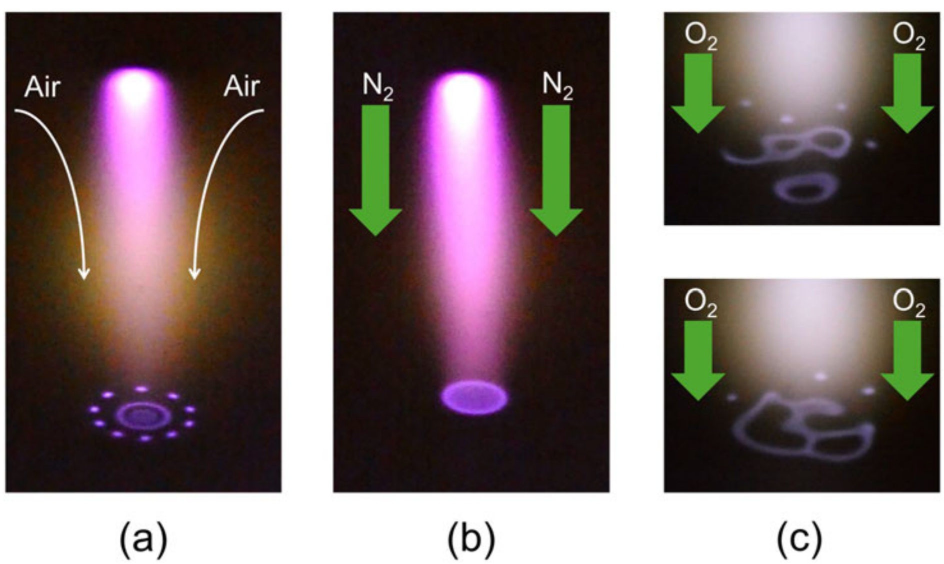

Figure 2. Example images of the discharge and the pattern formation. (a)The pattern forms when the discharge is generated in ambient air. (b)The pattern never forms when the discharge is generated with the nitrogen sheath gas. (c)The pattern changes when the discharge is generated with the oxygen sheath gas.

3. Results

3.1. The dependence of the ratio of the helium gas to oxygen gas on the pattern formation

Figure 3 shows images of the discharge and the pattern observed above the anode at the discharge currents of 30, 50, 70 mA with an electrodes distance of 12 mm (a)when the anode is liquid and (b)when the anode is metal, respectively. The helium gas flow rate was changed between 150-400 sccm, and the helium gas flowed in ambient air (composed of approximately 21 % oxygen). The radial spread of the pattern became smaller as the helium gas flow rate increased, and the pattern also had a larger radial spread and complex structure as the discharge current increased. When the patterns formed, dark region was observed between the anode surface and the positive column. These trends were similar for both cases in liquid anode and metal anode. A movie of changes in the pattern formation when the helium gas flow increased from 150 sccm to 350 sccm is shown in the supplementary data.

The changes in discharge voltage when the discharge current was increased between 20-80 mA using liquid and metal as the anode and helium flow rates between 150-400 sccm, respectively, are shown in Fig. 4(a) and Fig. 4(b). Both liquid anode and metal anode showed negative characteristics, in which the discharge voltage decreased as the discharge current increased. The discharge voltage decreased from 1.5 kV to 1.0 kV at the discharge currents of 20-80 mA and was almost constant at the discharge currents of 40 mA and higher. There was no significant difference in the voltage-current characteristics for the different helium gas flow rates, and the results were approximately similar.

Figure 5 shows images of the discharge and the pattern observed above the anode at the helium gas flow rates of 200, 300, 400 sccm with an electrodes distance of 12 mm when 1000 sccm flow rate of oxygen sheath gas flows around the discharge, and the anode is (a)liquid and (b)metal, respectively. The discharge current was increased between 20-80 mA. Similar to the conditions under which the discharge was generated in ambient air shown in Fig. 3, the radial spread of the pattern became larger and its structure became more complex as the helium gas flow rate was smaller and the discharge current was higher. Supplementary data shows a movie of the pattern formation changes when helium gas flow rate is increased. Two discharge modes with different brightness of the positive column were observed. Only the bright mode of the positive column was observed when the current was increased under the condition of helium gas flow rate of less than 200 sccm. However, under conditions of helium gas flow rates higher than 200 sccm, the dark mode of the positive column was observed at low currents, and as the current was increased, the mode changed from dark to bright. The pattern of dots and the pattern composed of curves were formed above the anode in the bright mode and the dark mode, respectively.

The voltage-current characteristics of the discharge using liquid and metal as the anode with the oxygen sheath gas flowing around the discharge are shown in Fig. 6(a)

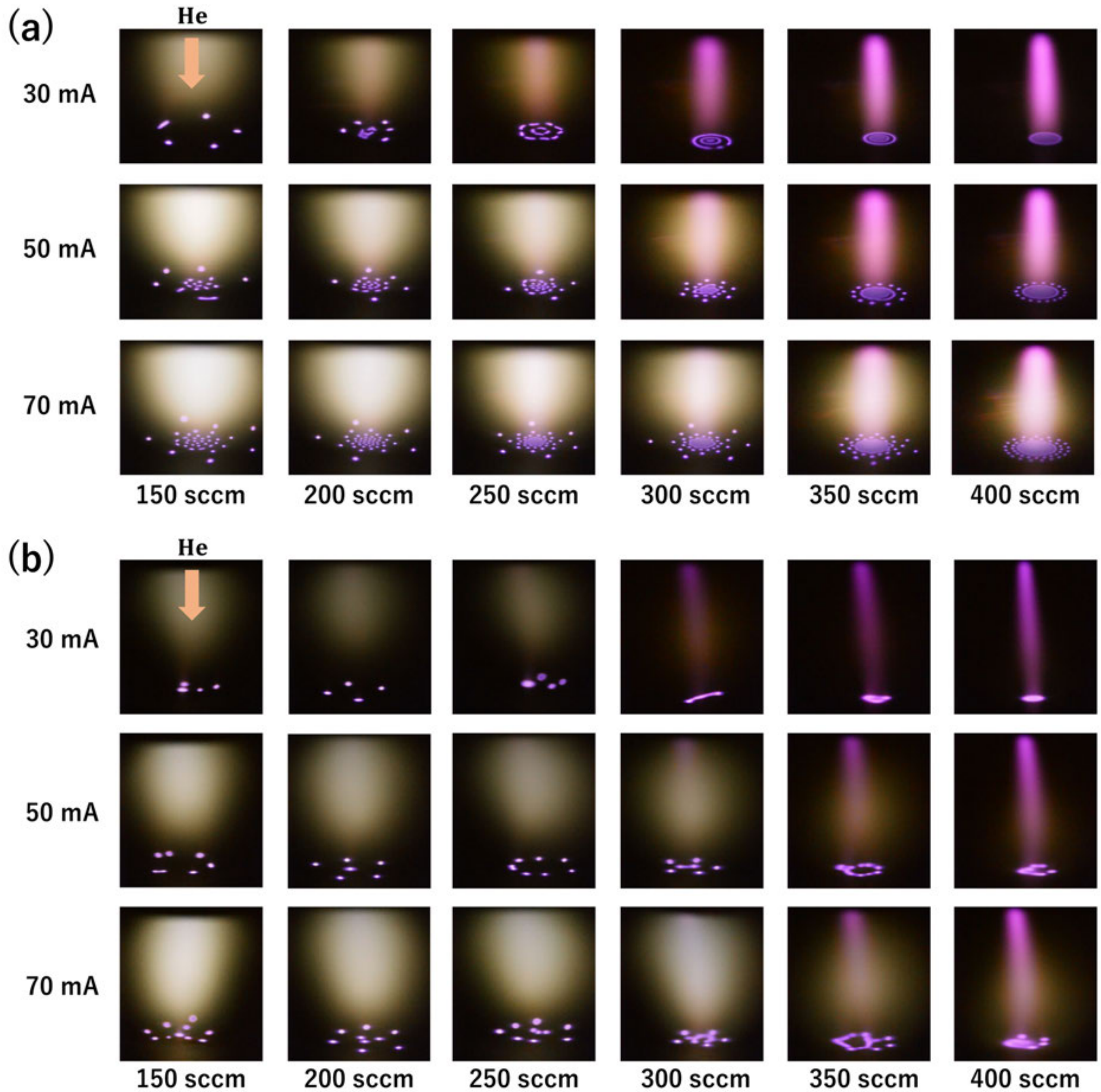

Figure 3. Dependence of the helium gas flow rate in the discharge center on the pattern formation. (a)When liquid is used as anode. (b)When a metal rod is used as anode.

and Fig. 6(b), respectively. The discharge current was increased between 20-80 mA, and the helium gas flow rate was changed between 150-400 sccm. There were differences in the voltage-current characteristics for the different helium gas flow rates when the oxygen sheath gas was flowing around the discharge column. At the discharge current of 20 mA, the discharge voltages were approximately 1.2-1.3 kV and 1.0-1.1 kV when the helium gas flow rates were 150-200 sccm and when 250-400 sccm, respectively. However, the voltages in all cases of the helium gas flow rates became the approximate same value of 1.1 kV when the current increased to 80 mA. In both the cases of the liquid and metal anode, the discharge voltage slightly decreased when the helium gas rates were

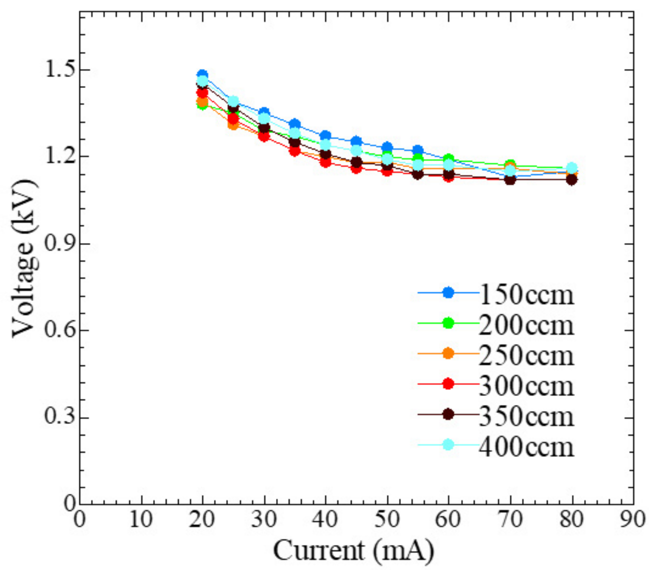

(a)

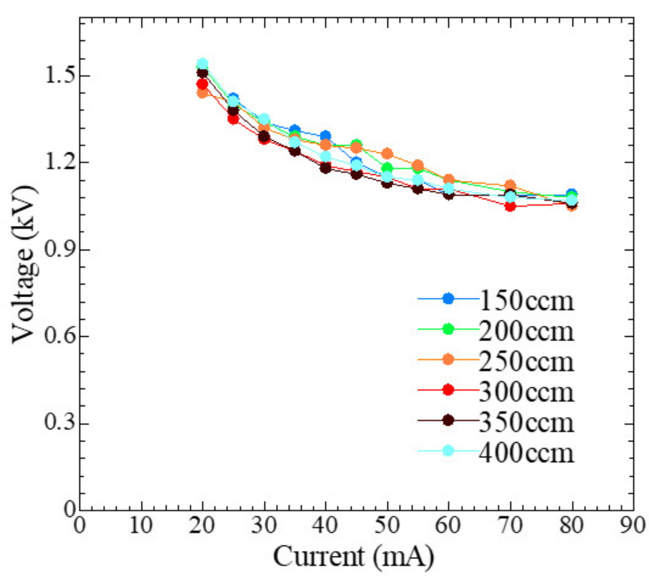

(b)

Figure 4. Voltage-current characteristics of the discharges which are generated in ambient air (without the sheath gas). (a)When liquid is used as anode. (b)When a metal rod is used as anode.

150 and 200 sccm between 20-80 mA. The voltage of the 250 sccm helium gas flow rate increased between 20-30 mA and became similar change to the voltages of the 150 and 200 sccm helium gas flow rates over 30 mA. The voltages of the 300 sccm in the liquid anode and the 300-400 sccm in the metal anode were roughly constant between 20-50 mA and became similar changes to the voltages of the 150-250 sccm helium gas flow rates over 50 mA. The voltages of the 350 and 400 sccm in the liquid anode were roughly constant at 1.0 kV between 20-60 mA and increased to approximately 1.1 kV over 60

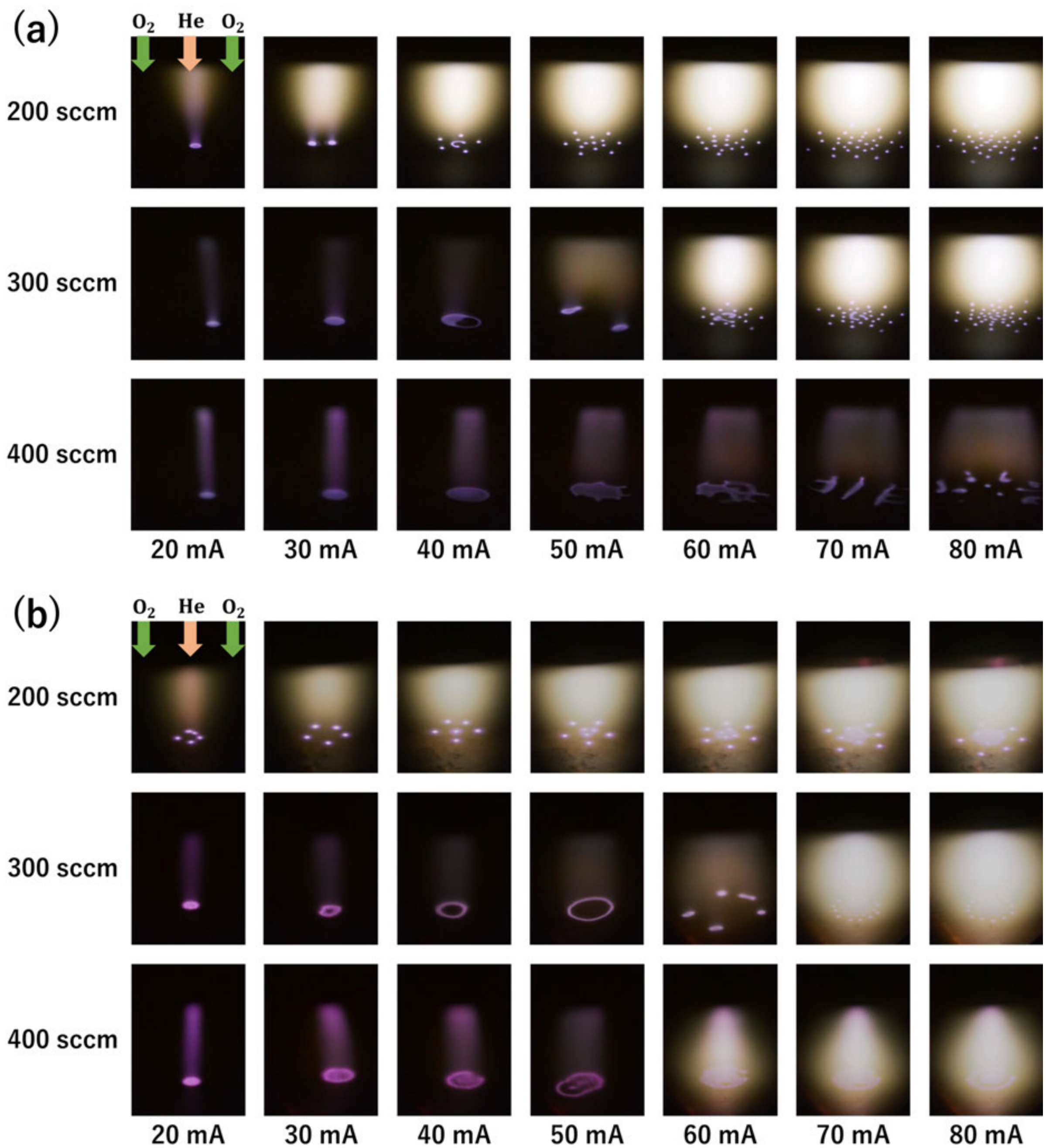

Figure 5. Dependence of pattern formation on the Helium gas flow rate in the discharge center when 1000 sccm flow rate of oxygen gas flows around the discharge column (a)When liquid is used as anode. (b)When metal plate is used as anode.

mA. Then, comparing the image in Figure 4 with the graph in Figure 5, it can be seen that the bright and dark discharge mode of the positive column corresponds to plots on the line with a high voltage value of approximately 1.2 kV and plots on the line with a low voltage value of approximately 1.0 kV, respectively.

As shown in Fig. 3 and Fig. 5, we observed various discharge modes with changing the gas flow rates of helium gas and using oxygen sheath gas. Figure 7 shows optical

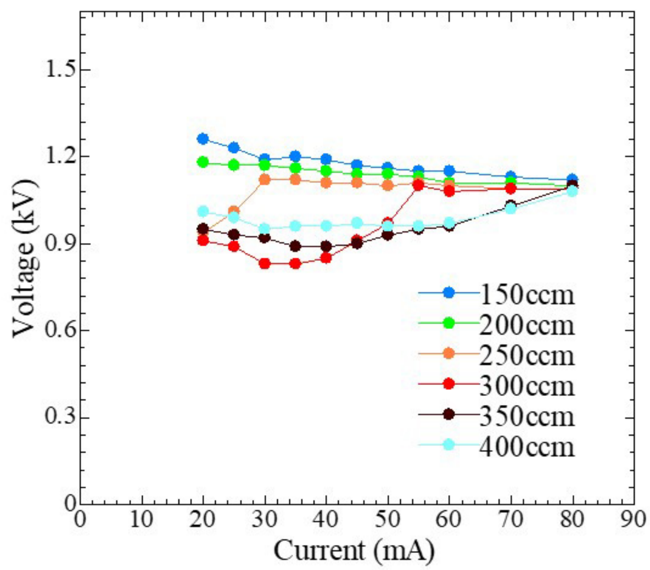

(a)

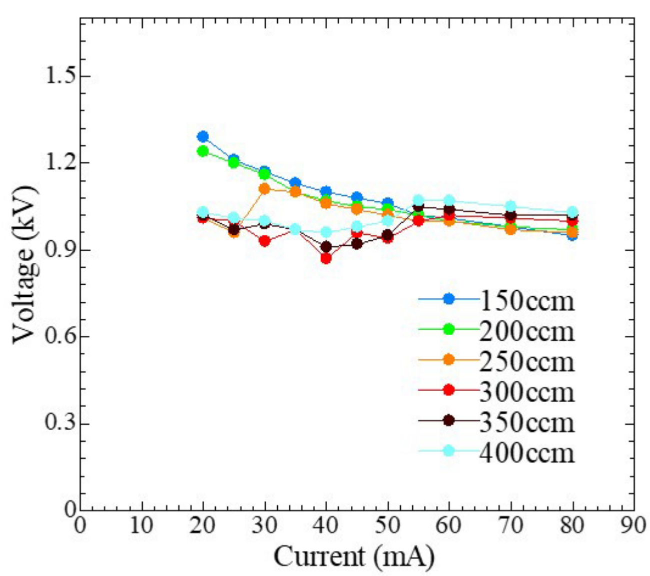

(b)

Figure 6. Voltage-current characteristics of the discharges with the oxygen sheath gas. (a)When liquid is used as anode. (b)When a metal rod is used as anode.

emission spectra from the typical discharge modes observed in the case of liquid anode, and the focused points were at the pattern area and the positive column area 5 mm above the anode. The flow rates of helium gas were 200 sccm ((a), (b)) and 400 sccm ((c), (d)), and 1000 sccm flow rate oxygen sheath gas was flowing in (b) and (d). The distance between the electrodes and the discharge current were fixed at 12 mm and 50 mA, respectively. In the case of the helium gas flow rate of 200 sccm shown in Figures 7(a) and (b), the light emission from the pattern area was mainly N_2 (second positive system) and OH (A-X), but the light emission from the positive column area was mainly only OH (A-X). The optical emission of atomic helium and atomic hydrogen were also observed, and the optical emission of atomic oxygen was observed when the oxygen sheath gas was flowing. In addition, the optical emssion of molecular NO_2, which appeared in the images shown in Fig. 7(a) and (b) as the white halo was observed as a continuous spectrum at wavelengths of 450-700 nm from the positive column area. In the case of the helium gas flow rate of 400 sccm shown in Figures 7(c) and (d), the light emission from both the pattern area and the positive column area was mainly N_2 (second positive system) and OH (A-X). The optical emission intensities of N_2 and OH were smaller when oxygen sheath gas was flowed, and the optical emission of atomic oxygen was observed. The spectra shown in Fig. 7 were obtained when the liquid anode was used, and we obtained similar spectra when the metal anode was used.

3.2. Measurements of temperature distribution in and around the discharge

Figure 8 shows images of the OH radical rotational temperature distribution measured by the LIF method. The discharges were generated in ambient air with 300 sccm helium gas flow, and the distance between electrodes and current values were (a)4 mm, 40 mA, (b)7 mm, 20 mA, (c)10 mm, 20 mA, (d)7 mm, 40 mA, (e)10 mm, 40 mA and (f)10 mm, 60 mA, respectively. The patterns did not form under the conditions of (a), (b) and (c), but formed under the conditions of (d), (e) and (f). The color range bar for the rotational temperature of OH radicals is shown in the upper right corner of Fig. 8, corresponding to 0-3000 K from black to white. The area where the OH radicals were present in the image is circled by dotted lines, and the rotational temperature inside this area could be obtained. Under the conditions in which the patterns did not form as in (a), (b), and (c), the temperature of the discharge area was approximately 1500-2000 K, whereas under the conditions in which the patterns formed as in (d), (e), and (f), the temperature of the discharge area was approximately 3000 K.

Figure 9 also shows images of the OH radical rotational temperature distribution with the same color range bar shown in Fig. 8, and the discharges in Fig. 9 were generated with the (a), (b)oxygen sheath gas or (c), (d)nitrogen sheath gas. The distance between electrodes was fixed at 10 mm, and the current values were (a), (c)40 mA and (b), (d)60 mA. The gas flow rates of helium and oxygen or nitrogen sheath gas were 300 and 1000 sccm, respectively. The patterns formed under the conditions of (a) and (b) which the discharge was generated with the oxygen sheath gas, but did not form under the conditions of (c) and (d) which with the nitrogen sheath gas. Under the conditions with oxygen sheath gas and the pattern formation, the temperature of the discharge area was approximately 2500 K at (a)40 mA, and approximately 3000 K at (b)60 mA. On the other hand, under the conditions with nitrogen sheath gas and no pattern formation, the temperature of the discharge area was approximately 2500 K at both (c)40 mA and (d)60 mA.

In addition to the LIF method, we also used Rayleigh scattering to investigate temperature of the discharge area. Figure 10 shows example images of Rayleigh scattering signal obtained by the irradiation of the pulsed 532 nm laser beam which was focused by the focal length f=20 cm lens. In all three images in Fig. 10, the distance between electrodes was fixed at 10 mm, and Fig. 10(a), (b), and (c) show no discharge generation, the condition of discharge generated at the 20 mA current and at 60mA, respectively. The laser beam was irradiated at a height of 2 mm from the surface of the liquid anode shown in Fig. 10(a), and we were able to obtain the Rayleigh scattering signal in the area where the laser passed through. The Rayleigh scattering signals shown in Fig. 10(b), and (c) are the combined images obtained by six laser irradiation at 2 mm from the liquid anode surface and at different heights from there by 1 mm. From these images shown in Fig. 10, it was visualized that during discharge generation, the Rayleigh scattering signal was decreased in the discharge area.

Figure 11(a) shows a graph of Rayleigh scattering signal intensity obtained in Fig. 10 on the vertical axis and position on the horizontal axis, with the center of the discharge at the position of 10 mm. Rayleigh scattering signal intensities shown in Fig. 11 were obtained at a height of 2 mm from the liquid anode surface, and the “Air” (black line), “10 mm 20 mA” (green line) and “10 mm 60 mA” (red line) in Fig. 11 correspond to (a), (b), and (c) in Fig 10, respectively. Figure 11(a) also shows the “5 mm 40 mA” (blue line) condition as a shorter distance between electrodes without the pattern formation, and this Rayleigh scattering signal was obtained from a position 2 mm above the liquid anode as well.

Figure 11(b) shows the Rayleigh scattering signals in Fig. 11(a) converted to temperature, and the conversion calculation was performed as follows. First, we assumed that the pressure p is constant at atmospheric pressure (=1013 hPa), which means the particle number density n and gas temperature T are inversely proportional to each other from the relationship p=nkT (where k is Boltzmann’s constant). Then, since the intensity of the Rayleigh scattering signal I is proportional to the particle number density n ($I \propto n$), I is inversely proportional to temperature($I \propto 1/T$). Assuming that the temperature T_{Air} is constant at 300 K in ambient air without discharge, the following relationship is derived.

$$T_{\mathrm{Discharge}} = \frac{I_{\mathrm{Air}}}{I_{\mathrm{Discharge}}} \times T_{\mathrm{Air}} = \frac{I_{\mathrm{Air}}}{I_{\mathrm{Discharge}}} \times 300[\mathrm{K}],$$

where, I_{Air} and $I_{\mathrm{Discharge}}$ are the intensities of Rayleigh scattering signal in ambient air and under the condition that the discharge is generated. This is how we estimated the gas temperatures under the conditions of the discharge generation. Under the condition of ”10 mm 60 mA” which the pattern formation was observed, the gas temperature was approximately 3000 K at the center of the discharge with 3-mountainous shapes temperature distribution. On the other hand, under the other discharge conditions (”10 mm 20 mA” and ”5 mm 40 mA”) with no pattern formation, the gas temperature of the discharge center was approximately 2000 and 1500 K, respectively. These results were in good agreement with the temperatures obtained from the rotational temperatures of OH radicals measured by the LIF method shown in Fig. 8.

The gas temperatures were also investigated when the oxygen or nitrogen sheath gas flowed around the discharge. Figure 12(a) and (b) show the estimated gas temperatures converted from the Rayleigh scattering signal intensities when the discharge was generated with (a)oxygen sheath gas and (b)nitrogen sheath gas, which are the same discharge conditions to Fig. 9. The gas temperature of the discharge center was approximately 2500 K at (a)40 mA, and approximately 3000 K at (b)60 mA under the conditions with oxygen sheath gas and the pattern formation. In contrast, the gas temperature of the discharge center was approximately 2500 K at both (c)40 mA and (d)60 mA. Focusing on the gradient of the graph, (a)with the oxygen sheath gas, the gradient was gradual near the top of the mountain and steep outside. On the other hand (b)with the nitrogen sheath gas, the top of mountain was sharp, and the gradient outside was more gentle than that of (a)oxygen sheath gas. These results were also in agreement with the temperatures obtained from the rotational temperatures of OH radicals measured by the LIF method shown in Fig. 9.

3.3. Influence of electro-negative gases other than oxygen gas on the pattern formation

The pattern formation can be observed when the discharge is generated in ambient air or the oxygen sheath gas is flowed around discharge as shown in Fig. 2. It has been found that the presence of oxygen gas is important for the pattern formation, and the significant role of oxygen gas in plasmas may be thought to be ingredient of negative ions because oxygen gas is one of the electro-negative gases. Therefore, we investigated influence of electro-negative gases other than oxygen gas on the pattern formation. Figure 13 shows example images of the discharges when SF_6 gas or CO_2 gas was used as the sheath gas. We generated the discharge at the current of 20-60 mA with 200-300 sccm of helium gas, and the flow rate of SF_6 or CO_2 sheath gas was 1000-2000 sccm. Supplementary data shows a movie of the pattern formation changes when SF_6 sheath gas was flowed. Here, it is noted that nitrogen gas was used to dilute the SF_6 gas concentration to a few % for our safety, and this experiment was conducted in a drafter. The CO_2 sheath gas was used in ambient air. As a result of these experiments, the pattern formation was not observed above the anode when discharges were generated under these conditions. The dark region between the anode surface and the positive column which was observed when the pattern formed in Figs. 3 and 5 was also not observed under these conditions.

4. Discussion

The experimental results show that the pattern structure clearly changes depending on the ratio of helium gas and oxygen gas. The trends of pattern formation and discharge voltage-current characteristics were similar when the current and the helium gas flow rate were changed for both liquid and metal anodes. These results suggest that the mechanism of pattern formation is fundamentally the same when liquid or metal is used as the anode. The difference in pattern between liquid and metal anodes is thought to be caused by differences in conductivity and surface smoothness between liquid and metal. For example, if the surface of the metal anode is scratched, the current is more likely to be concentrated in the scratched spot, and the spread of the pattern will be smaller. In addition, changes in metal surface conditions due to oxidation of the metal surface caused by discharge generation often affected the current concentration. On the other hand, since the liquid anode surface is entirely smooth, the pattern above the liquid anode is thought to be point-symmetrical. It should be noted that in the case of the liquid anode, the pattern structure also depends on the liquid conductivity or the kind of electrolyte.

The main component of the light emission from the self-organized pattern area above the anode surface is mainly nitrogen, even if the gas ratio changes. When the surrounding gas is air, the anode column has predominantly pink light emission, but the main component of this light emission is from nitrogen. As the current increases, a white light emission is observed, which is the optical emission of NO_2. The continuous light emission from NO_2 is observed at 450-700 nm, as shown in Fig. 7, and similar spectra were reported in study of NO_2 Fluorescence [44]. NO_2 is observed due to the temperature rise caused by the discharge from nitrogen and oxygen in the air. This light emission has also been observed in other DC discharges, and it has been reported that the discharge spreads radially more in an air atmosphere than in a nitrogen atmosphere [45]. When the oxygen sheath gas is flowed, the light emission of the positive column area becomes weaker at low currents. Under this condition, the discharge maintaining voltage is low. As the current increases, the positive column area becomes thicker, and the white light emission of NO_2 is observed, forming a pattern similar to that in air. Under this condition, the discharge maintaining voltage becomes high.

In the cases of many discharge plasmas generated in ambient air, the self-organized luminous pattern formation is observed as the current increases, and the white light emission of NO_2 is observed in this case [6, 7, 28, 29]. The light emission of NO_2 is observed when the helium gas flow rate becomes lower compared to the same discharge current, and this is expected to be due to the increasing admixture of surrounding gases into the discharge area which has the center helium gas flow. Although there have been no reports that discuss the correlation between the light emission from the positive column area and the self-organized luminous pattern, experimental results show that the pattern formation is easily observed when the NO_2 is observed and the positive column spreads in the radial direction. It has been reported that air plasma has a higher temperature than nitrogen plasma in atmospheric-pressure DC discharges, and the radial spread may be due to a decrease in the gas density at the discharge center. On the other hand, when the helium gas flow rate is higher, the discharge does not spread in the radial direction because the discharge is generated along the center helium gas flow. In this case, the pattern formation is unlikely to be observed.

Simulation studies on the self-organization in discharges have shown that pattern structures can theoretically be obtained by taking even the radial spread into account

[46], and the results in this study suggest that the radial spread of the discharge is important for pattern formation. The pattern formation may be affected by not only the anode surface but also the entire discharge. In other words, the results in this study may suggest that the conditions of whether or not the pattern is formed are determined by the entire plasma, whereas the pattern structure depends on the conductivity of the liquid or the surface condition of the metal.

We obtained the temperatures in two different ways, by the LIF of OH and by Rayleigh scattering, and these two results were in good agreement, therefore, the temperatures we obtained in this study can be considered reliable. Previous studies have shown that the formation of self-organized patterns in atmospheric pressure DC glow discharges is more likely to occur with a larger distance between electrodes (> about 5 mm) and larger current (> about 30 mA) [6,7]. In this study, it was found that under conditions where patterns form, the temperature was as high as 2500-3000 K, which was higher than the temperature under conditions where patterns do not form. As shown in Fig. 3, 5 and 7, light emission of NO_2 was observed, which could be one of the evidence for the high temperatures in the discharge, such as 2500-3000 K. This is because NO_2 is a kind of thermal NOx, which is produced in such a high temperature environment [47].

The graph shape of the temperature distribution was different for discharges in ambient air, discharges with the oxygen sheath gas and discharges with the nitrogen sheath gas, and the gradient of the temperature change was steeper under the conditions where the pattern formed. This fact may suggest that not only the high temperature of the discharge, but also the large gradient of the temperature change has an important influence on the pattern formation. The presence of oxygen gas may have the effect of increasing the temperature and altering the temperature gradient in the discharge. In fact, studies comparing temperatures in atmospheric pressure DC glow discharges in ambient air and nitrogen atmosphere have reported higher temperatures in air ambient discharges [48,49]. In arc discharges, it has been reported that air discharges have higher input power than nitrogen discharges [50], which may indicate that the temperature is also higher in the air discharges. Higher gas temperatures in atmospheric pressure plasmas cause a decrease in gas number density, which may reproduce the same situation as the pattern formation in low-pressure plasmas [21–23]. In addition, it was also reported that pattern formation was observed in atmospheric pressure DC discharge in pure helium gas by increasing the current to a few amperes [51]. This may suggest that the self-organized pattern formation in atmospheric pressure plasma and that in low-pressure plasma may have the similar mechanism of the pattern formation. The detailed mechanism is not yet clear, but the distribution of temperature or gas density at the center of the discharge may affect the diffusion in the reaction-diffusion system.

We have been considering that the role of oxygen gas in the pattern formation may be the effect of generating negative ions in the plasma and that the negative ions may play a significant role in the pattern formation. However, there is still no evidence that negative ions are involved in the pattern formation. To the contrary, as shown in Fig. 13, no pattern formation was observed when SF_6 gas or CO_2 gas, electronegative gases other than oxygen gas, were flowed around the discharge as sheath gases as well as oxygen gas. This fact may suggest the presence of oxygen gas is undoubtedly important for the pattern formation, but it is doubtful that negative ions are important. It should be noted, however, that the possibility that the negative ion density in the plasma is a key of the pattern formation cannot be completely eliminated, because the electron attachment cross-sections are different between oxygen, SF_6 and CO_2 [52–55], and negative ion densities that are expected to be generated in this study were not aligned for quantitatively comparison.

5. Conclusions

In this work, we investigated the influence of gas conditions and gas temperature in the discharge on the pattern formation observed above the anode. We used both the liquid anode and the metal anode, and the trends of changes in the pattern formation by changing the discharge current and the helium gas flow rate were similar. The trends were also similar when the oxygen sheath gas flowed around the discharge. In addition, we found that the gas temperature in the discharge was higher under the conditions where the pattern formed than that without the pattern formation. The gradient of the temperature in the discharge may be also important for the pattern formation because the temperature gradient of the discharge with the pattern formation was steeper than that of the discharge without the pattern formation. There is no doubt that oxygen gas has a significant effect on the formation of the self-organized luminous pattern in atmospheric pressure DC glow discharge, but further investigation is needed to identify whether this effect is due to negative ions or other factors. Considering the radial spreading of the NO_2 light emission region in the positive column with increasing current and temperature, the radial spreading of the discharge plasma and higher temperature in the discharge (or its temperature gradient) are important for the pattern formation above the anode.

Acknowledgment

This work is supported by JSPS KAKENHI 23KJ0048 and 23H01388.

References

[1] P. Bruggeman and C. Leys 2009 J. Phys. D: Appl. Phys. **42** 053001
[2] B. R. Locke, M. Sato, P. Sunka, M. R. Hoffmann and J.-S. Chang 2006 Ind. Eng. Chem. Res. **45** 882-905
[3] N. Shirai, S. Uchida and F. Tochikubo 2014 Jpn J. Appl. Phys. **53** 046202
[4] N. Shirai, K. Ichinose, S. Uchida and F. Tochikubo 2011 Plasma Sources Sci. Technol. **20** 034013
[5] N. Shirai, G. Suga and K. Sasaki 2020 Plasma Sources Sci. Technol. **29** 025007
[6] N. Shirai, S. Ibuka and S. Ishii 2009 IEEE Ttans. Appl. Phys. Express. **2** 036001
[7] N. Shirai, S. Uchida and F. Tochikubo. 2014 Plasma Sources Sci. Technol. **23** 054010

[8] J. P. Trelles 2016 J. Phys. D: Appl. Phys. **49** 393002
[9] J. E. Foster, Y. E. Kovach, J. Lai and M. C. Garcia 2020 Plasma Sources Sci. Technol. **29** 034004
[10] A. M. Turing 1952 Phil. Trans. R. Soc. **237** 37
[11] S. Kondo and R. Asai 1995 Nature **376** 765
[12] A. Nakamasu, G. Takahashi, A. Kanbe and S. Kondo 2009 Proc. Natl. Acad. Sci. U.S.A. **106** 8429
[13] S. Kondo and T. Murai 2010 Science **329** 1616
[14] J. Nagumo, S. Arimoto and S. Yoshizawa 1962 Proc. IRE **50** 2061
[15] N. Kopell and L. N. Howard 1973 Studies in Applied Mathematics **52** 291
[16] B. Pokroy, S. H. Kang, L. Mahadevan and J. Aizenberg 2009 Science **323** 237
[17] A. N. Zaikin and A. M. Zhabotinskii 1970 Nature **225** 535
[18] V. Petrov, V. Gaspar, J. Masere and K. Showalter 1993 Nature **381** 240
[19] P. Rumbach, A. E. Lindsay and D. B. Go 2019 Plasma Sources Sci. Technol. **28** 105014
[20] M. S. Bieniek, P. G. C. Almeida and M. S. Benilov 2018 Plasma Sources Sci. Technol. **27** 05LT03
[21] K. H. Schoenbach, M. Moselhy1 and W. Shi 2004 Plasma Sources Sci. Technol. **13** 177
[22] W. Zhu, P. Niraula, P. G. C. Almeida, M. S. Benilov and D. F. N. Santos 2014 Plasma Sources Sci. Technol. **23** 054012
[23] S. Nasuno 2003 Chaos **13**, 1010–1013
[24] P. Bruggeman, J. Liu, J. Degroote, M. G. Kong, J. Vierendeels and C. Leys 2008 J. Phys. D: Appl. Phys. **41** 215201
[25] T. Verreycken, P. Bruggeman and C. Leys 2009 Journal of Applied Physics **105** 083312
[26] A. Wilson, D. Staack, T. Farouk, A. Gutsol, A. Fridman and B. Farouk 2013 Plasma Sources Sci. Technol. **17** 045001
[27] S. Y. Miao, C. S. Ren, D. Z. Wang, Y. T. Zhang, B. Qi and Y. N. Wang 2008 IEEE Trans. Plasma Sci. **36** 126
[28] Y. E. Kovach, M. C. Garcia and J. E. Foster 2019 IEEE Trans. Plasma Sci. **47** 3214
[29] Y. E. Kovach, M. C. Garcia and J. E. Foster 2021 Plasma Sources Sci. Technol. **30** 015007
[30] Z. Yang, Y. Kovach and J. Foster 2021 J. Appl. Phys. **129** 163303
[31] P. Zheng, X. Wang, J. Wang, B. Yu, H. Liu, B. Zhang and R. Yang 2014 Plasma Sources Sci. Technol. **24** 015010
[32] S. Zhang and T. Dufour 2018 Physics of Plasmas **25** 073502
[33] T. Srivastava, M. S. Simeni, G. Nayak and P. J. Bruggeman 2022 Plasma Sources Sci. Technol. **31** 085010
[34] X. Li, S. Zhou, K. Gao, J. Ran, K. Wu and P. Jia 2022 IEEE Trans. Plasma Sci. **50** NO. 6, pp. 1717-1722
[35] X. Qin, B. Feng, R. Wang, Y. Ma, Q. Zhang and X. Zhong 2023 Plasma Process Polym. **21** e2300055
[36] N. Shirai, S. Uchida, F. Tochikubo and S. Ishii 2011 IEEE Trans. Plasma Sci. **39** 2652
[37] Y. E. Kovach, F. Zhang, F. Gao and J. E. Foster 2019 J. Vac. Sci. Technol. **A** **37** 011301
[38] M. S. Benilov 2008 Phys. Rev. **E** **77** 036408
[39] P. G. C. Almeida, M. S. Benilov, M. D. Cunha and M. J. Faria 2009 J. Phys. D: Appl. Phys. **42** 194010
[40] P. G. C. Almeida, M. S. Benilov and M. J. Faria 2010 Plasma Sources Sci. Technol. **19** 025019
[41] H. Ishigame, S. Nishiyama and K. Sasaki 2015 Jpn. J. Appl. Phys. **54** 01AF02.
[42] K. Sasaki, H. Ishigame and S. Nishiyama 2015 Eur. Phys. J. Appl. Phys. **71** 20807.
[43] N. Shirai, H. Owada and K. Sasaki 2021 Plasma Sources Sci. Technol. **30** 125012.
[44] K. Sakurai AND H. P. Broida 1969 J. Chem. Phys. **50** 2404–2410
[45] X. Duten, D. Packan, L. Yu, C. O. Laux and C. H. Kruger 2002 IEEE Trans. Plasma Sci. **30** NO. 1, pp. 178-179
[46] M. S. Benilov 2014 Plasma Sources Sci. Technol. **23** 054019
[47] S. K. Hoekman and C. Robbins 2012 Fuel Processing Technology **96** 237–249
[48] D. Staack, B. Farouk1, A. Gutsol and A. Fridman 2008 Plasma Sources Sci. Technol. **17** 025013

[49] K. Tomita, K. Urabe, N. Shirai, Y. Sato, S. Hassaballa, N. Bolouki, M. Yoneda, T. Shimizu and K. Uchino 2016 Jpn. J. Appl. Phys. **55** 066101
[50] L. Yu, X. Li, X. Tu, Y. Wang, S. Lu and J. Yan 2010 J. Phys. Chem. A **114** 360–368
[51] V. I. Arkhipenko, Th. Callegari, Y. A. Safronau, L. V. Simonchik and I. M. Tsuprik 2013 Plasma Sources Sci. Technol. **22** 045003
[52] W. R. Henderson, W. L. Fite and R. T. Brackmann 1969 Phys. Rev. **183** 157
[53] L. M. Chanin, A. V. Phelps and M. A. Biondi 1962 Phys. Rev. **128** 219
[54] L. G. Christophorou and J. K. Olthoff 2001 International Journal of Mass Spectrometry Volume **205** Issues 1–3
[55] E. Carbone, W. Graef, G. Hagelaar, D. Boer, M. M. Hopkins, J. C. Stephens, B. T. Yee, S. Pancheshnyi, J. van Dijk and L. Pitchford 2021 Atoms **9** 16

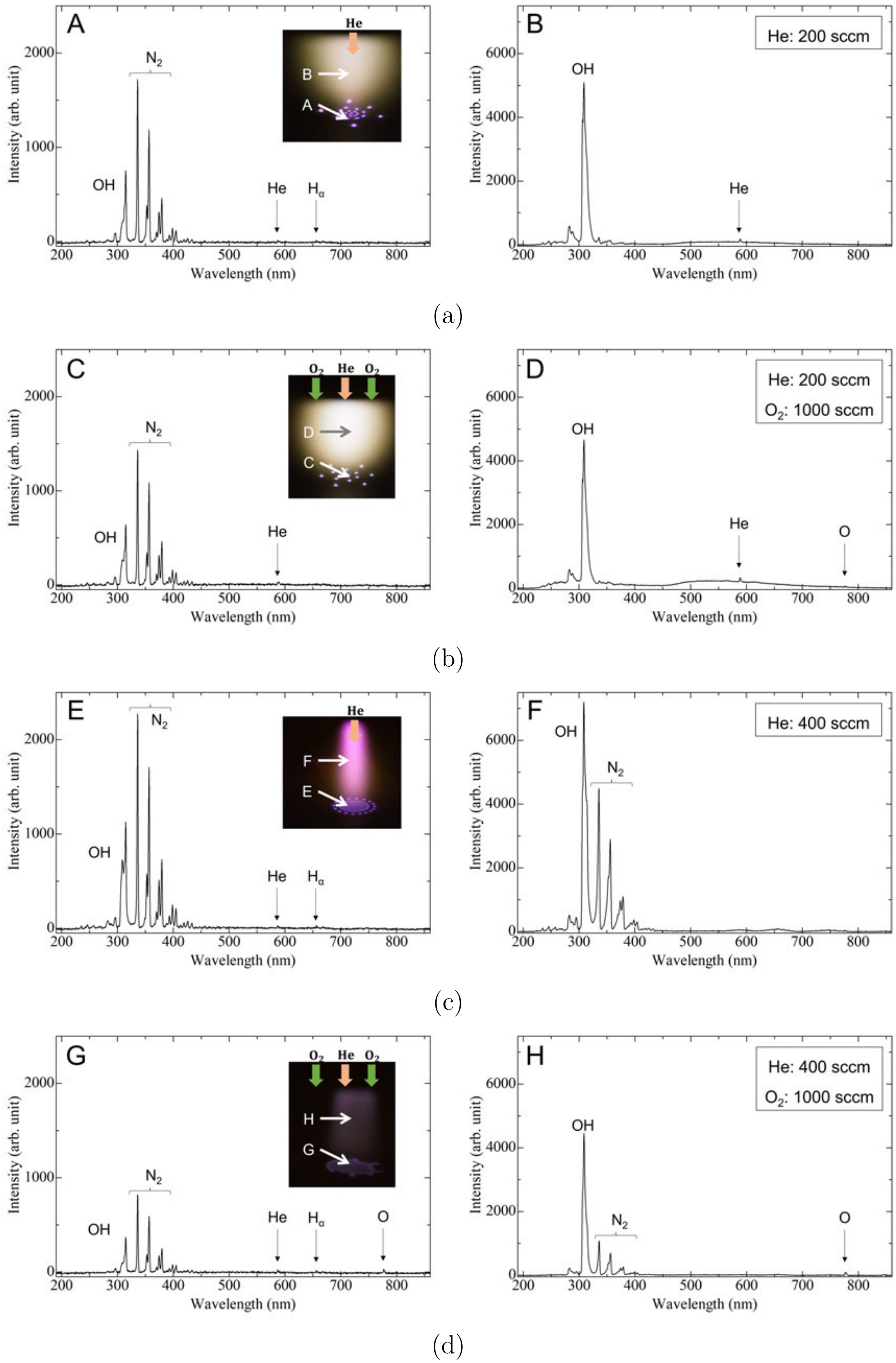

Figure 7. Optical emission spectra from the discharge with the pattern formation. The flow rates of helium gas were (a), (b)200 sccm and (c), (d)400 sccm, and 1000 sccm flow rate oxygen sheath gas was flowing in (b) and (d). The distance between the electrodes and the discharge current were fixed at 12 mm and 50 mA, respectively.

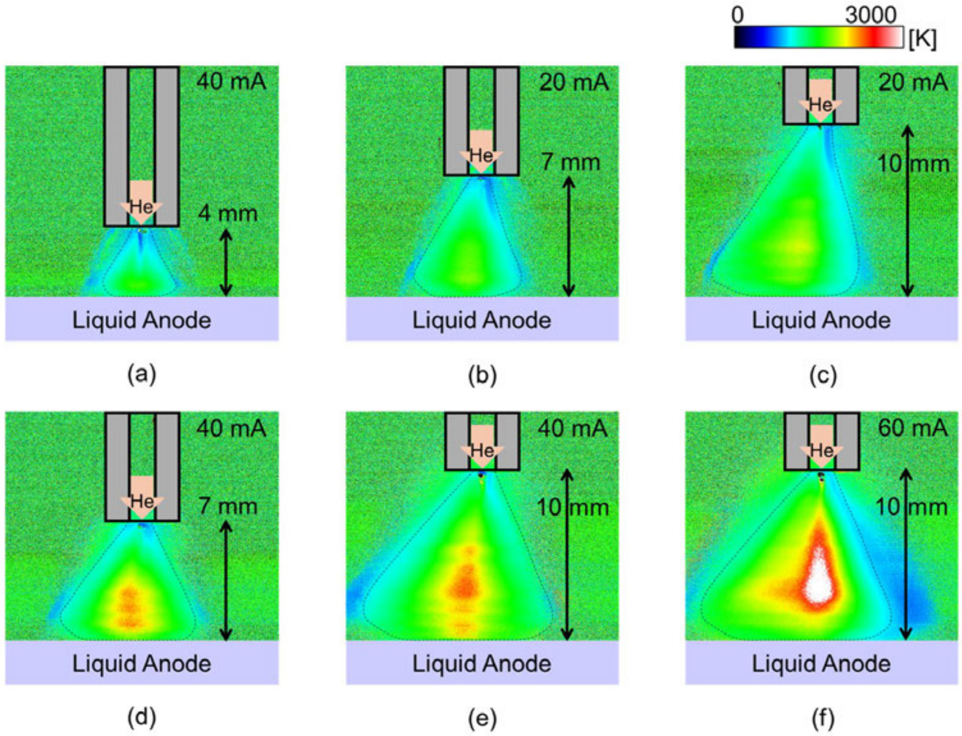

Figure 8. Images of the OH radical rotational temperature distribution. Discharges were generated in ambient air, and the distance between electrodes and current values were (a)4 mm, 40 mA, (b)7 mm, 20 mA, (c)10 mm, 20 mA, (d)7 mm, 40 mA, (e)10 mm, 40 mA and (f)10 mm, 60 mA, respectively.

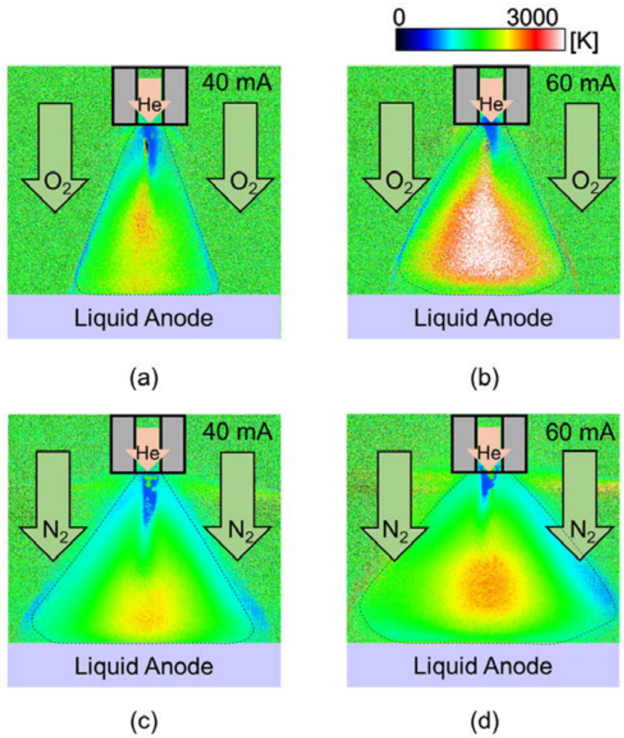

Figure 9. Images of the OH radical rotational temperature distribution. Discharges were generated with the (a), (b)oxygen or (c), (d)nitrogen sheath gas. The distance between electrodes was fixed at 10 mm. The current values were (a), (c)40 mA and (b), (d)60 mA.

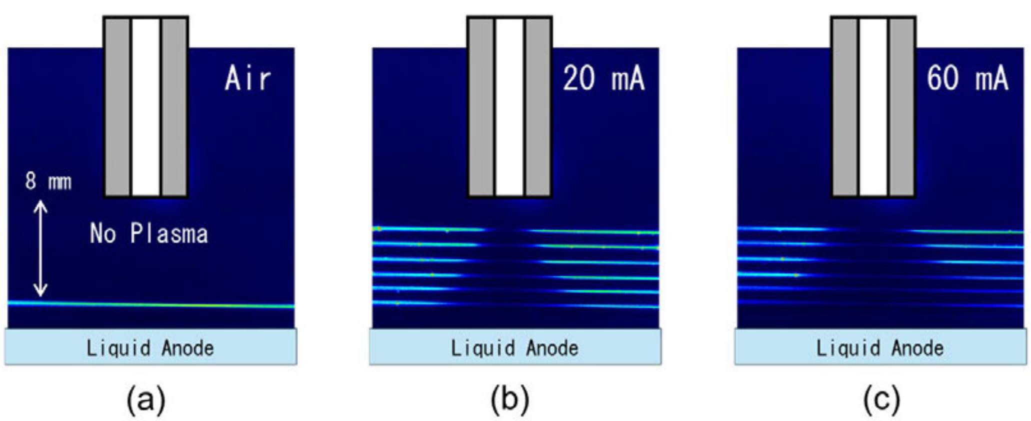

Figure 10. Example images of Rayleigh scattering signal from (a)only air, (b)the discharge at the current of 20 mA and (c)60 mA.

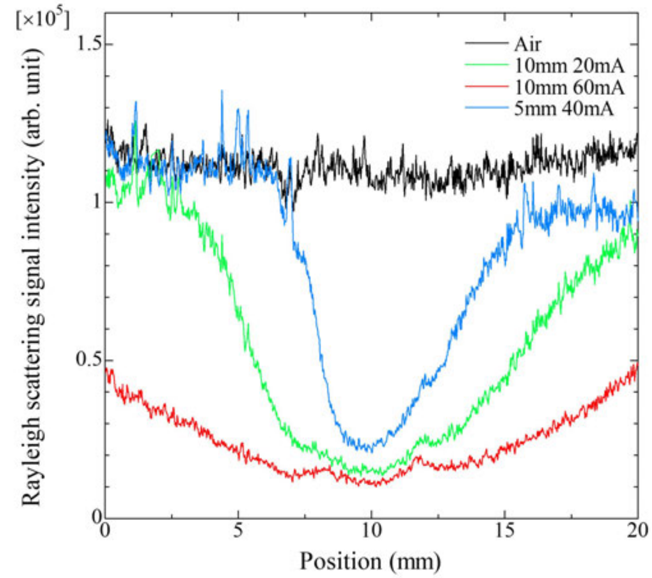

(a)

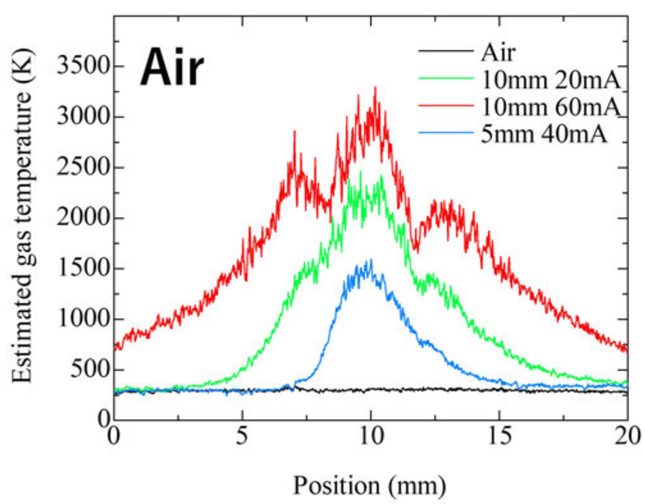

(b)

Figure 11. (a)Intensities of Rayleigh scattering signal and (b)estimated gas temperature converted from Rayleigh scattering signal.

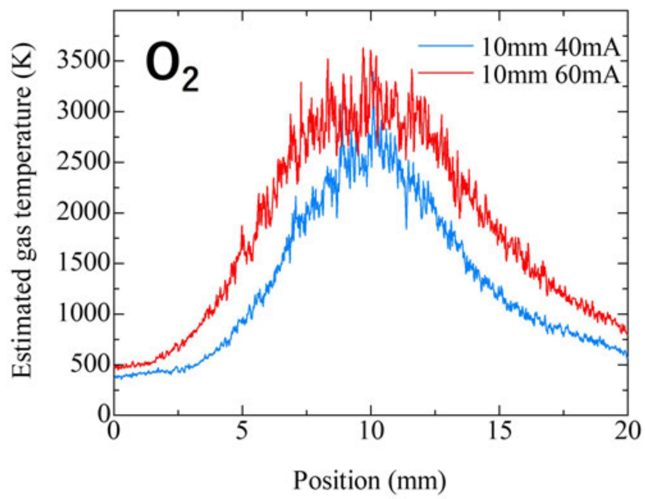

(a)

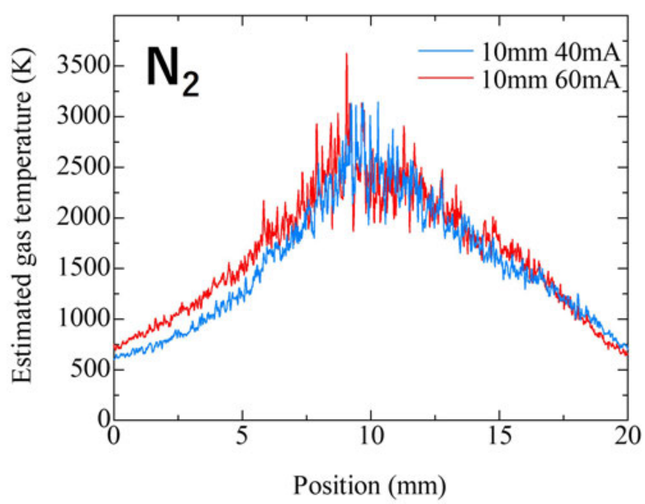

(b)

Figure 12. Estimated gas temperature converted from Rayleigh scattering signal when the discharge was generated with (a)oxygen sheath gas and (b)nitrogen sheath gas.

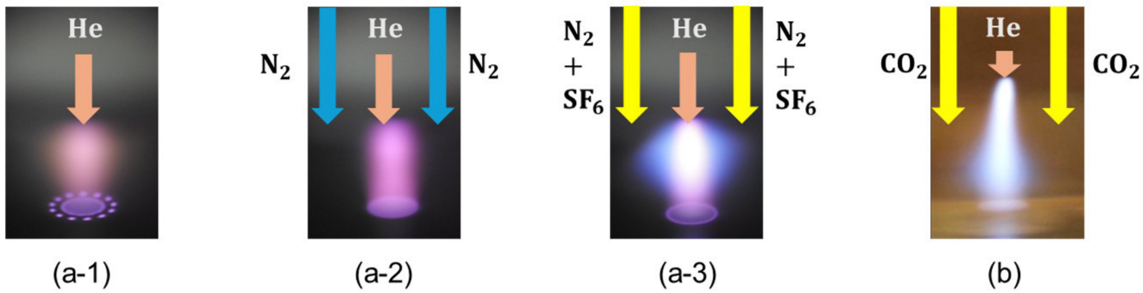

Figure 13. Example images of the discharges when SF_6 gas or CO_2 gas was used as the sheath gas. (a-1)Initial condition which only helium gas was flowed, and the pattern formed above the liquid anode, (a-2)nitrogen sheath gas started to flow, and the pattern disappeared, (a-3)a few % of SF_6 gas added into the nitrogen sheath gas, and the pattern was not still observed. Here, it is noted that nitrogen gas was used to dilute the SF_6 gas concentration for our safety, and this experiment was conducted in a drafter. (b)CO_2 gas was flowed as the sheath gas, and the pattern was not observed.